
The Gaussian-Multinoulli Restricted Boltzmann Machine

A Potts Model Extension of the GRBM

Nikhil Kapasi

Electrical and Computer Engineering
University of California, Santa Barbara
Santa Barbara, CA 93117
nkapasi@ucsb.edu

William Whitehead

Electrical and Computer Engineering
University of California, Santa Barbara
Santa Barbara, CA 93117
williamwhitehead@ucsb.edu

Luke Theagarajan

Electrical and Computer Engineering
University of California, Santa Barbara
Santa Barbara, CA 93117
1usthe@ucsb.edu

Abstract

Many real-world tasks, from associative memory to symbolic reasoning, demand discrete, structured representations that standard continuous latent models struggle to express naturally. We introduce the Gaussian-Multinoulli Restricted Boltzmann Machine (GM-RBM), a generative energy-based model that extends the Gaussian-Bernoulli RBM (GB-RBM) by replacing binary hidden units with q -state Potts variables. This modification enables a combinatorially richer latent space and supports learning over multivalued, interpretable latent concepts. We formally derive GM-RBM’s energy function, learning dynamics, and conditional distributions, showing that it preserves tractable inference and training through contrastive divergence. Empirically, we demonstrate that GM-RBMs model complex multimodal distributions more effectively than binary RBMs, outperforming them on tasks involving analogical recall and structured memory. Our results highlight GM-RBMs as a scalable framework for discrete latent inference with enhanced expressiveness and interoperability.

1 Introduction

Restricted Boltzmann Machines (RBMs) constitute a class of undirected energy-based models defined on a bipartite graph between visible units \mathbf{v} and latent units \mathbf{h} (hidden). Their tractable block Gibbs updates [6] and scalable approximate inference via contrastive divergence enable efficient training on high-dimensional datasets [1, 6]. In the binary hidden configuration, an RBM reduces to an Ising model where hidden units $h_j \in -1, +1$ interact pairwise through couplings W_{ij} , yielding an energy landscape analogous to classical spin systems [14]. The Gaussian–Bernoulli RBM (GB-RBM) augments this formulation by replacing these visible variables with Gaussian potentials, while preserving binary hidden spins [7]. Although GB-RBMs capture continuous inputs such as image intensities or sensor readings, the binary latent constraints limit their expressivity when representing multimodal or discrete feature correlations [4, 15].

The q -state Potts model generalizes the Ising model by allowing each spin s_j to occupy one of q discrete states, enriching the model’s capacity to encode complex interaction patterns and phase

transitions [22, 32]. Potts-type energy functions have demonstrated efficacy in image segmentation, combinatorial optimization, community detection, and categorical embedding tasks, where capturing higher-order discrete structures is key [12]. Building on these principles, we introduce the Gaussian–Multinoulli Restricted Boltzmann Machine (GM-RBM), which integrates Gaussian-distributed visible units with a hidden layer of q -state Potts spins. This GB-RBM-like architecture provides a clear path to benchmarking and showcasing the power of Potts-based energy functions.

The Gaussian–Multinoulli Restricted Boltzmann Machine (GM-RBM) we propose has a small change in the underlying representation of hidden nodes that has a profound improvement on model performance. While prior work has addressed mixed-variate inputs using Gaussian–Bernoulli structures [26], convolutional and tiled weight-sharing schemes for spatial hierarchies [10], and implicit mixture models of RBMs for multimodal density estimation [20], these approaches retain binary or sigmoidal-based latent representations, limiting their ability to capture categorical variation at the feature level. In contrast, the GM-RBM replaces binary hidden units with q -state Potts (Multinoulli) variables, enabling each hidden unit to express one of several discrete latent modes rather than mere presence or absence. This yields a latent space that scales as q^m (with m hidden units), and facilitates more structured, interpretable, and compositional generative behavior. Unlike energy-based models that treat discrete latents as auxiliary sampling artifacts [4], or continuous latent embeddings for mixed data [25], the GM-RBM directly leverages categorical latent dynamics to build rich distributions over continuous-valued visible units. This hybrid formulation opens new avenues for modeling structured analog data, such as trajectories, natural images, or biophysical time series, with discrete control over generative features.

2 Background and Model Overview

2.1 Background and Motivation

Restricted Boltzmann Machines (RBMs) have played a foundational role in energy-based modeling and unsupervised representation learning. In particular, Gaussian–Bernoulli RBMs (GB-RBMs), which pair real-valued Gaussian visible units with binary latent variables, have been adopted for modeling continuous input data such as images and signals [15]. However, while GB-RBMs are capable of learning low-level features, they face inherent limitations in their ability to capture structured, discrete latent representations.

The root of this limitation lies in the mismatch between the binary latent space and the Gaussian visible manifold. The Gaussian prior enforces a continuous energy landscape in the input space, which, when combined with binary latent units, leads to the learning of clustered, overlapping encodings. These encodings tend to coalesce into fuzzy representations that lack the expressiveness needed for capturing discrete abstractions, such as object parts, symbolic states, or multimodal feature variants.

Moreover, the binary latent units in GB-RBMs act as on/off switches, providing limited control over the diversity and structure of the hidden space. This bottleneck hampers the model’s ability to disentangle categorical or compositional structure, particularly when the data exhibits rich semantic variation.

2.2 Motivating Discrete Latent Structure: Potts Units

In contrast, Potts models, which extend binary variables to q -state categorical variables, offer a compelling mechanism for reintroducing structured discrete latent representations into energy-based models. By allowing each hidden unit to express one of multiple mutually exclusive states, Potts units can represent discrete modes, templates, or symbolic features directly. This increases the combinatorial capacity of the model from 2^m (binary) to q^m (categorical), enabling richer and more interpretable feature representations.

Importantly, Potts units also induce a sharper factorization of latent structure, allowing for the emergence of compositional encodings where different latent units capture orthogonal or complementary concepts. This categorical structure aligns more naturally with real-world semantics and improves both generalization and controllability.

2.3 The Gaussian-Multinoulli RBM (GM-RBM)

To address the limitations of GB-RBMs and exploit the representational advantages of Potts variables, we introduce the Gaussian-Multinoulli Restricted Boltzmann Machine (GM-RBM). In this architecture, the visible layer consists of Gaussian-valued units, modeling real-valued data such as sensor signals or pixel intensities while the hidden layer consists of Multinoulli (Potts) units, each of which selects one of q discrete latent states.

Each Potts state corresponds to a different “template” or filter that contributes to the energy of the model, allowing a single hidden unit to encode latent modes or feature classes rather than just presence/absence. The GM-RBM thus combines the smooth representational power of Gaussian inputs with the symbolic richness of discrete latent categories.

This hybrid construction restores the model’s ability to capture structured, discrete latent features while retaining flexibility in modeling continuous-valued observations. As we show, the GM-RBM can learn more interpretable latent spaces, support combinatorial recombination of features, and exhibit sharper mode separation in the visible manifold than its Gaussian-Bernoulli counterpart.

3 Theoretical Foundations of the Gaussian-Multinoulli RBM (GM-RBM)

The Gaussian-Multinoulli Restricted Boltzmann Machine (GM-RBM) extends the classical Gaussian-Bernoulli RBM by replacing binary latent units with discrete q -state Potts (Multinoulli) variables. This modification introduces a combinatorially structured latent space capable of expressing discrete modes while modeling continuous-valued data in the visible layer. In this section, we develop a mathematical understanding of how this architecture supports richer and more structured representations.

3.1 Energy Function and Architecture

The GM-RBM defines a joint energy over visible variables $v \in \mathbb{R}^n$ and hidden Potts variables $h = (h_1, \dots, h_m)$, where each $h_j \in \{1, \dots, q\}$ selects a discrete state for hidden unit j :

$$E(v, h) = \frac{1}{2} \sum_{i=1}^n (v_i - b_i)^2 - \sum_{j=1}^m c_{j, h_j} - \sum_{i=1}^n \sum_{j=1}^m W_{ij}^{(h_j)} v_i \quad (1)$$

This can be re-expressed in terms of the conditional Gaussian mean $\mu(h)$ as:

$$E(v, h) = \frac{1}{2} \|v - \mu(h)\|^2 + \text{const}(h), \quad \text{where} \quad \mu(h) = b + \sum_{j=1}^m W_j^{(h_j)} \quad (2)$$

Each hidden unit contributes a state-specific template vector $W_j^{(h_j)}$, and the visible layer is modeled as a Gaussian centered at the compositional mean $\mu(h)$:

$$P(v | h) = \mathcal{N}(\mu(h), I) \quad (3)$$

3.2 Compositionality and Factored Representation

The mean vector $\mu(h)$ is a sum over learned templates selected by the Potts states:

$$\mu(h) = b + \sum_{j=1}^m W_j^{(h_j)} \quad (4)$$

This creates a structured and factored representation in visible space. Each hidden unit encodes one of q possible modes, and the overall visible configuration is a compositional sum of these latent components. This modularity enables reuse of latent features across samples, disentangled latent representation, and combinatorial expressivity across q^m configurations

The set of all compositional means $\mu(h)$ forms a structured lattice in \mathbb{R}^n . The resulting energy landscape has the following properties:

- **Locally linear:** Each mode defines a Gaussian with fixed covariance
- **Globally discrete:** The mode structure is defined by a combinatorial Potts lattice
- **Modular:** Latent units contribute independently to the visible pattern

This structure allows GM-RBMs to model multimodal distributions over continuous space with precise symbolic control via latent discrete selections.

4 Hetero-associative Memory

Hetero-associative memory refers to a system’s capability to learn paired associations between distinct patterns, allowing the retrieval of a target pattern (e.g., a response word) when presented with a corresponding stimulus (e.g., a cue word) [11, 19]. This concept, rooted in cognitive modeling and neural computation, was further explored by Hinton in 1981 [2] and later employed in language-related tasks using Gaussian-Bernoulli Restricted Boltzmann Machines (GB-RBMs) [27]. However, the binary hidden units of GB-RBMs impose a hard ceiling on representational capacity.

Across the board, GM-RBMs deliver consistently higher recall than GB-RBMs, with gains amplifying at larger q and corpus sizes even when the number of parameters were identical between the two models. It is important to note that this performance gain is obtained although the GM-RBM was trained using only *Gibbs sampling*, while the GB-RBM used a stronger and more expensive hybrid Gibbs-Langevin Sampling.

4.1 Experimental Setup

4.1.1 Dataset

We replicated the experimental setup in Tsutsui and Hagiwara, constructing a word-pair dataset representing conceptual relationships (e.g., "apple is-a fruit") [27]. We randomly selected pairs from WordNet [28], excluding compound or incomplete entries and sampled 500-3,000 word pairs to create smaller datasets for training and testing scalability.

Each word pair is treated as a directional association task and encoded as a concatenated embedding vector [17], mirroring the hetero-associative memory objective of recalling a target concept from a given stimulus.

4.1.2 Preprocessing

We trained a 200-dimensional Continuous Bag of Words (CBOW) Word2Vec model [18] on the word-pair dataset (100 iterations, window size 5, no frequency cutoff). We normalized each vector dimension to zero mean and unit variance to mitigate small-magnitude issues. For each stimulus-response pair, embeddings were concatenated to form a 400-dimensional input vector for the RBM’s visible layer.

4.1.3 Computational Setup

We used a compute node (Intel Xeon Gold 6154 $\times 2$, 512 GB RAM, NVIDIA Tesla P40) running Red Hat Enterprise Linux 8. Models were trained with CUDA-accelerated PyTorch (v1.13) on a single GPU. Experiments were automated via a modular framework for data loading, configuration, visualization, and checkpointing.

4.1.4 Training

Our GM-RBM learned to associate stimulus–response word embeddings. Datasets comprised semantically related word pairs (e.g., doctor–nurse, sun–light). Following a similar procedure to Tsutsui and Hagiwara [27], we trained a CBOW Word2Vec model [23] on these two-word sentences to capture in-domain semantics, producing 200-dimensional embeddings (100 iterations, window size 5, no frequency cutoff).

We normalized each embedding dimension to zero mean and unit variance to avoid numerical instability. The stimulus and response embeddings were concatenated into a 400-dimensional visible layer vector.

We trained the GB-RBM using contrastive divergence with a two-step Gibbs burn-in, employing the more expensive Gibbs–Langevin sampling procedure. In contrast, the GM-RBM variant relied solely on standard Gibbs sampling, reducing computational overhead. Notably, in the special case of $q = 2$, the GM-RBM formulation becomes almost equivalent to the GB-RBM: the only difference is that in the GB-RBM, the two weight matrices are essentially negatives of one another. Hidden-unit counts were scaled inversely with the number of Potts states to keep capacity constant. Training used Adam (LR = 10^{-4}) with mini-batches of 64. We evaluated recall by inferring responses via Gibbs sampling and selecting the nearest neighbor; accuracy was the percentage of correct matches.

We stopped training early when recall accuracy reached 0.98 on the validation set, when the standard deviation of validation accuracy over 20 checkpoints fell below 0.01, or when no improvement was observed for 10 consecutive checkpoints.

4.2 Results

To isolate the effect of the Potts hidden units, we did two key tests. The first was a parameter-matched comparison where the total number of weights was kept equal while q was increased. This ensured that any observed gains in recall accuracy arise purely from the richer Potts representation. The second was a similar sweep where q was held constant while the number of hidden units themselves was increased. Both sweeps were done across varying dataset sizes, measuring the accuracy of the recall in pairs embedded in Word2Vec [18].

Each marker in Figures 1 and 2 denotes an independently trained model using identical early-stopping criteria. Error bars have been omitted as the observed performance gains were uniformly large, making statistical uncertainty negligible for the comparative trends shown.

For data shown in Figure 1, it is important to note that the total number of parameters was held constant i.e. hidden layers were decreased proportionally to the cardinality of the Potts state q (See 1).

It is also important to note $q = 2$ for the GM-RBM is a case of the Potts nodes where weights do not have to be constrained i.e. negatives of one another. The original GB-RBM outperforms the GM-RBM for $q = 2$, possibly due to the lack of this constraint. Despite the GM-RBMs being trained using the simpler Gibbs update, the $q = 4, 6, 8, 10$ GM-RBM models all vastly outperform the GB-RBM, which used the more expensive Gibbs-Langevin update [15].

Since constraining the total number of parameters to be identical might obfuscate the potential of both models, we swept the number of hidden nodes and dataset sizes as shown in Figure 2. It can be clearly seen that GM-RBM $q = 2$ and the GB-RBM both fail when $N > 2000$, while the GM-RBM $q = 4$ maintains its retrieval accuracy.

4.2.1 Parameter matched q sweep

To empirically showcase the direct effect of the additional Potts states, we held the total number of model parameters constant while varying the number of Potts states q , isolating the effect of the state space’s structure on hetero-associative performance. Figure 1 plots retrieval accuracy against the number of associative pairs in the training set for each q . For the binary case $q = 2$, the GB-RBM with Gibbs–Langevin sampling maintains near-perfect accuracy at small dataset sizes but collapses sharply beyond 1000 pairs, whereas the GM-RBM using only Gibbs sampling degrades more rapidly. In contrast, models with higher state cardinality ($q = 4, 6, 8, 10$) sustain almost perfect retrieval up to roughly 1200–1500 pairs and exhibit a more gradual decline as a function of the dataset size(N). Notably, $q = 10$ consistently outperforms lower- q configurations even for large N .

To keep the model capacity fixed across different Potts-state configurations, we solve for the number of hidden units n_h by dividing the total budget of weight parameters n_w by the size of each hidden Potts spin q . Since each hidden unit with q Potts states contributes q weight vectors of length equal to the number of visible units n_v , then number of hidden units is given by

$$n_h = \lceil \frac{n_w}{n_v} \times q \rceil \quad (5)$$

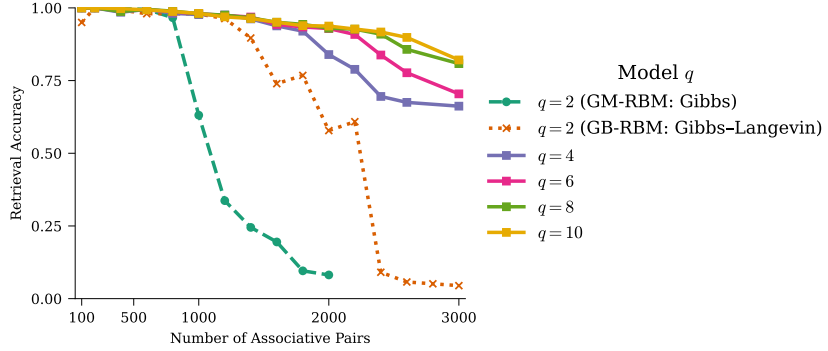


Figure 1: Retrieval accuracy versus the number of associative pairs for different numbers of Potts states (q) in a parameter-matched GB-RBM and GM-RBM setup

We chose $n_w = 800,000$, ensuring that the binary case $q = 2$ matched the optimal hidden-unit count of 1,000 reported by Tsutsui and Hagiwara [27] for the GB-RBM. This ensures that, as we increase the number of Potts states k , we reduce the number of hidden units proportionally so that every model has the same total number of parameters.

Table 1: Potts-state q versus number of hidden units

	$q = 2$	$q = 4$	$q = 6$	$q = 8$	$q = 10$
Hidden Units	1000	500	333	250	200

This result demonstrates increasing the number of discrete states enhances memory robustness under constant parameter constraints. By allocating representational capacity across more Potts states, the model tolerates larger associative loads, suggesting an optimal trade-off point around moderate state sizes (e.g., $q = 6$ or 8) for typical dataset scales in the 2000–2500 pair range.

4.2.2 Hidden nodes sweep

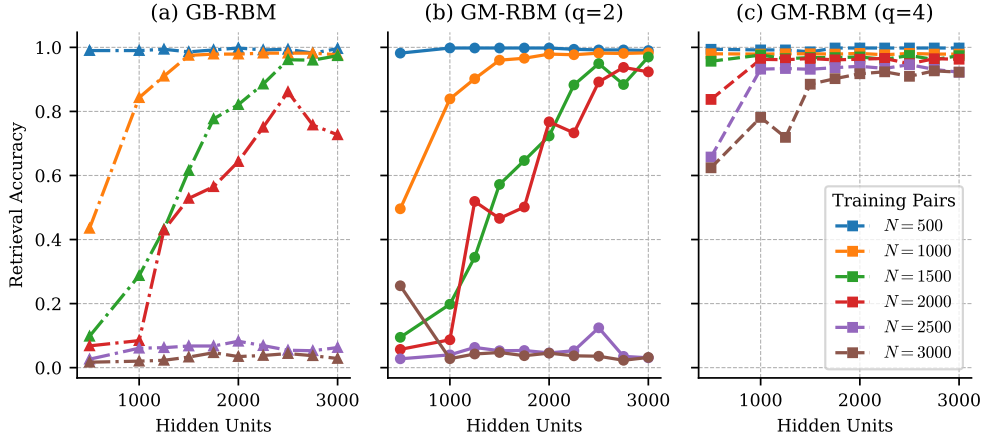


Figure 2: Retrieval accuracy on a semantic hetero-associative memory task as a function of hidden-layer size for different model variants and dataset sizes. (a) GB-RBM (Gibbs–Langevin Update), (b) GM-RBM with $q = 2$ (Gibbs Update), and (c) GM-RBM with $q = 4$ (Gibbs Update). Each curve corresponds to a different number of training word-pair examples (N).

In order to showcase how varying the hidden-layer dimensionality affects retrieval performance across dataset sizes, we swept the number of hidden units from 500 to 3000 while fixing the state cardinality

q . Figure 2 presents retrieval accuracy curves for three models: a standard Gaussian–Bernoulli RBM (GB-RBM), a GM-RBM with $q = 2$, and a GM-RBM with $q = 4$. Each curve represents a different dataset size ($N = 500, 1000, 1500, 2000, 2500, 3000$ associative word pairs).

For the binary GM-RBM ($q = 2$), accuracy is near-perfect at small loads but degrades sharply as N increases, recovering only when hidden units exceed 1500. In contrast, the Potts-based GM-RBM with $q = 4$ maintains over 90% accuracy across all dataset sizes with just 1000 hidden units. The GB-RBM baseline requires roughly 2500 hidden units to achieve similar performance at large scales (e.g., $N = 2500$).

These findings demonstrate a clear trade-off between hidden-layer dimensionality and state complexity: increasing q substantially lowers the hidden-unit requirement for robust associative recall, yielding a more parameter-efficient memory architecture.

5 Auto-associative memory

As a "proof-of-concept" to demonstrate the generative capability of our GM-RBM, we performed a replication of the generative experiments from the original GB-RBM paper [15]. On MNIST, we trained for 500 epochs, and on CelebA for 100 epochs. Starting from i.i.d. Gaussian noise in the visible layer and running 1,000 steps of Gibbs sampling, we obtained samples (see Figure 3) that, by visual inspection, showcasing the GM-RBM's ability to still produce high-quality generative outputs.

5.1 Experimental setup

5.1.1 Datasets

We target two key datasets to showcase the GM-RBM's generative abilities: **MNIST** (28×28 grayscale handwritten digits) [13] and **CelebA** (Center-cropped and resized RGB facial images at 64×64 resolution) [16].

5.1.2 Preprocessing

All image datasets are normalized to zero mean and unit variance per channel [15]. CelebA images are center-cropped to 140×140 before downsampling to 64×64 [16]. The GMM datasets are constructed using predefined priors and covariance structures, allowing for exact density visualization and sampling [15]. For each dataset, we generate training and evaluation splits using standard protocols.

5.1.3 Computational resources

Experiments were performed on a dedicated compute node equipped with dual Intel Xeon Gold 5218 CPUs, 512 GB of RAM, and eight NVIDIA RTX 6000 GPUs connected via NVLink. All models were trained using CUDA-accelerated PyTorch (v1.13+) with single-GPU execution unless otherwise specified.

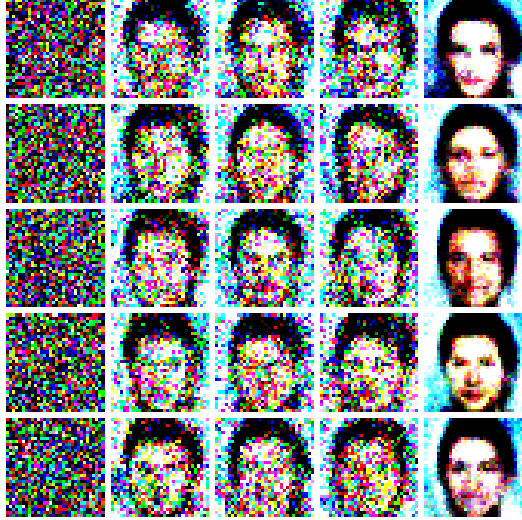
5.2 Results

We observe that the $q = 4$ GM-RBM begins to generate visually identifiable face/digit samples with an order of magnitude lower number of epochs compared to the GB-RBM trained with Gibbs–Langevin sampling (See Table 2. Although a fully controlled head-to-head comparison under identical hyperparameter budgets (see Table 2) requires further investigation (See Section 6.1, it is important to emphasize two key distinctions. Our GM-RBM relies solely on conventional Gibbs sampling, whereas Hinton's GB-RBM employs the more computationally expensive Gibbs–Langevin procedure [15]. This ability is most likely due to what the rapid mixing of Potts models compared to binary Boltzmann machines [22, 31, 32]. In addition, we maintain the same total number of parameters while increasing the number of Potts states.

This reduction in both sampling complexity and overall training budget underscores the richer latent representational capacity afforded by Potts-style hidden units, which can capture more nuanced multimodal structure with fewer resources. The stark difference in hyperparameters was chosen specifically to highlight the GM-RBM's ability to achieve high-quality samples under a dramatically reduced resource budget, showcasing its practical efficiency.



a Selected samples from MNIST



b Generation of CelebA images from random noise

Figure 3: Sampled results from GM-RBM of MNIST and CelebA datasets

Table 2: Hyperparameter settings for GB-RBM and GM-RBM on MNIST and CelebA

Hyperparameter	MNIST		CelebA	
	GB-RBM [15]	GM-RBM	GB-RBM [15]	GM-RBM
Number of states	2	4	2	4
Sampling style	Gibbs–Langevin	Gibbs	Gibbs–Langevin	Gibbs
Hidden nodes	4096	2048	10000	5000
Visible nodes	784	784	3072	3072
Epochs trained	3000	500	10000	100

6 Limitations and future work

While the Gaussian-Multinoulli Restricted Boltzmann Machine (GM-RBM) demonstrates improved expressiveness and recall performance over the binary GB-RBM, key limitations and future work remain.

6.1 Limitations of the current model

- 1. Sampling constraints:** In the current implementation, only Gibbs sampling is supported for the Potts-based GM-RBM. While this allows for tractable inference over discrete states, the absence of Langevin or hybrid Gibbs-Langevin samplers limits potential gains in sample quality and mixing speed. As q increases, the discrete state space grows, and relying solely on categorical sampling may lead to slower convergence or poor exploration of the energy landscape in more complex settings.
- 2. Evaluation domain:** The current evaluation focuses on word pair associations using Word2Vec embeddings. The generalization of GM-RBMs to other domains, such as vision, audio, or time series data, remains an open question and will require further validation. These limitations present valuable directions for future research, including scaling GM-RBMs to deeper architectures, optimizing discrete sampling methods, and exploring broader applications beyond associative memory tasks.
- 3. Epochs and training:** Currently, the GM-RBM is trained for a limited number of epochs (500 for MNIST, 100 for CelebA) to achieve initial convergence. While this rapid training demonstrates efficiency, it may not capture long-term stability or the potential benefits of extended training schedules. Optimal epoch budgets, early-stopping criteria, and the impact of prolonged training on sample diversity and model robustness are areas for further exploration.

6.2 Broader impact

6.2.1 Potts units in energy transformers

Energy Transformers (ETs) minimize a global energy via recurrent updates and have shown success in tasks such as image inpainting [9]. Replacing their binary hidden units with q -state Potts variables raises the latent capacity from 2^H to q^H , yielding:

$$E_{\text{mem}}(h) = - \sum_{\mu=1}^M \sum_{i=1}^H \delta(h_i, \xi_i^\mu) \quad (6)$$

where ξ^μ are stored patterns. Larger q reduces overlap between attractors, improving convergence selectivity. Embedding Gaussian–Potts RBMs into ETs may boost robustness and facilitate neuromorphic implementations; an empirical study of these hybrids is ongoing.

6.2.2 Extending DBMs to continuous data

Deep Boltzmann Machines (DBMs) stack Bernoulli–Bernoulli RBMs to learn hierarchical features via layer-wise Gibbs sampling and contrastive divergence [3, 24]. Their reliance on binary visibles limits real-valued inputs. As a front end, we propose a Gaussian–Potts energy:

$$E(v, h) = \sum_{i=1}^D \frac{(v_i - a_i)^2}{2\sigma_i^2} - \sum_{i,j} W_{ij}(v_i, h_j) - \sum_j b_{h_j}, \quad (7)$$

with $h_j \in 1, \dots, q$. This encoder maps \mathbb{R}^D into a q^H -state latent space, preserving DBM training while improving stability and expressiveness.

6.3 Bernoulli-Variable models and Potts benefits

Many foundational generative architectures rely on binary or Bernoulli units, including classical models like Bernoulli RBMs [6], Gaussian–Bernoulli RBMs [15], Deep Belief Networks [24], Deep Boltzmann Machines [3, 24], and Hopfield Networks. More recent advancements leveraging binary sampling mechanisms include Variational Autoencoders (VAEs) [5] with Bernoulli latents, Gumbel–Softmax VAEs [21] that provide differentiable relaxations for discrete sampling, Autoregressive Models such as PixelCNN [30] and PixelRNN [29] for sequential binary pixel generation, Binarized Neural Networks (BNNs) that constrain weights and activations to binary values, Latent Bernoulli Autoencoders [5] designed explicitly for compact binary representations, Spiking Neural Networks (SNNs) employing discrete spike events for communication, and Discrete Denoising Diffusion Models (D3PMs) [8] that extend diffusion processes to discrete data through multinomial transition kernels. Upgrading these binary units to Potts variables further increases representational granularity and sharpens attractor basins, significantly reducing interference among stored patterns and enabling richer discrete structures, ultimately enhancing the capability and expressiveness of associative and generative models.

6.4 Hardware-Efficient Implementation

Many of these models can be deployed with minimal overhead by leveraging sparse or event-driven representations (e.g., SPAD arrays [31]) and one-hot encoding of discrete states. Binary and Potts variables map naturally to bitwise logic and lookup tables, enabling FPGA, ASIC, and neuromorphic implementations with low memory footprint and energy consumption.

References

- [1] David H Ackley, Geoffrey E Hinton, and Terrence J Sejnowski. A learning algorithm for boltzmann machines. *Cognitive Science*, 9(1):147–169, 1985.
- [2] James A. Anderson and Geoffrey E. Hinton. *Parallel models of associative memory*. Lawrence Erlbaum Associates, Hillsdale, NJ, 1981.
- [3] Kyung Hyun Cho, Tapani Raiko, and Alexander Ilin. Gaussian-bernoulli deep boltzmann machine. In *The 2013 International Joint Conference on Neural Networks (IJCNN)*, pages 1–7, 2013.
- [4] Hanjun Dai, Rishabh Singh, Bo Dai, Charles Sutton, and Dale Schuurmans. Learning discrete energy-based models via auxiliary-variable local exploration. In *Advances in Neural Information Processing Systems*, volume 33, pages 10443–10455, 2020.
- [5] Jiri Fajtl, Vasileios Argyriou, Dorothy Monekosso, and Paolo Remagnino. Latent bernoulli autoencoder. In Hal Daumé III and Aarti Singh, editors, *Proceedings of the 37th International Conference on Machine Learning*, volume 119 of *Proceedings of Machine Learning Research*, pages 2964–2974. PMLR, 13–18 Jul 2020.
- [6] Geoffrey E Hinton. Training products of experts by minimizing contrastive divergence. Technical Report GCNU TR 2002-004, University College London, 2002.
- [7] Geoffrey E Hinton and Ruslan R Salakhutdinov. Reducing the dimensionality of data with neural networks. *Science*, 313(5786):504–507, 2006.
- [8] Jonathan Ho, Ajay Jain, and Pieter Abbeel. Denoising diffusion probabilistic models, 2020.
- [9] Benjamin Hoover, Yuchen Liang, Bao Pham, Rameswar Panda, Hendrik Strobelt, Duen Horng Chau, Mohammed J. Zaki, and Dmitry Krotov. Energy transformer. In *Advances in Neural Information Processing Systems*, volume 36, 2023.
- [10] Jyri Kivinen and Christopher K I Williams. Multiple texture boltzmann machines. In *Proceedings of the Fifteenth International Conference on Artificial Intelligence and Statistics*, volume 22 of *Proceedings of Machine Learning Research*, pages 638–646. PMLR, 2012.
- [11] B. Kosko. Bidirectional associative memories. *IEEE Transactions on Systems, Man, and Cybernetics*, 18(1):49–60, 1988.
- [12] Pik-Yin Lai and Yadin Y. Goldschmidt. Application Of Statistical Mechanics To Combinatorial Optimization Problems: The Chromatic Number Problem And Q Partitioning Of A Graph. 2 1987.
- [13] Yann LeCun, Léon Bottou, Yoshua Bengio, and Patrick Haffner. Gradient-based learning applied to document recognition. *Proceedings of the IEEE*, 86(11):2278–2324, 1998.
- [14] Yann LeCun, Sumit Chopra, Raia Hadsell, Marc’Aurelio Ranzato, and Fu-Jie Huang. A tutorial on energy-based learning. <https://www.cs.toronto.edu/~vnaier/ciar/lecun1.pdf>, 2006.
- [15] Renjie Liao, Simon Kornblith, Mengye Ren, David J. Fleet, and Geoffrey Hinton. Gaussian-bernoulli rbms without tears, 2022.
- [16] Ziwei Liu, Ping Luo, Xiaogang Wang, and Xiaoou Tang. Deep learning face attributes in the wild. In *Proceedings of the IEEE International Conference on Computer Vision (ICCV)*, pages 3730–3738, 2015.
- [17] Tomas Mikolov, Kai Chen, Greg Corrado, and Jeffrey Dean. Efficient estimation of word representations in vector space. In *Proceedings of the International Conference on Learning Representations (ICLR)*, 2013.
- [18] Tomas Mikolov, Kai Chen, Greg Corrado, and Jeffrey Dean. Efficient estimation of word representations in vector space, 2013.

- [19] Rafael Morales and Luis A. Pineda. Entropic hetero-associative memory, 2024.
- [20] Vinod Nair and Geoffrey E Hinton. Implicit mixtures of restricted boltzmann machines. In *Advances in Neural Information Processing Systems*, volume 21, pages 1145–1152. Curran Associates, Inc., 2008.
- [21] Sangshin Oh, Seyun Um, and Hong-Goo Kang. Recab-vae: Gumbel-softmax variational inference based on analytic divergence, 2022.
- [22] R. B. Potts. Some generalized order-disorder transformations. *Mathematical Proceedings of the Cambridge Philosophical Society*, 48(1):106–109, 1952.
- [23] Radim Řehůřek and Petr Sojka. Software Framework for Topic Modelling with Large Corpora. In *Proceedings of the LREC 2010 Workshop on New Challenges for NLP Frameworks*, pages 45–50, Valletta, Malta, May 2010. ELRA. <http://is.muni.cz/publication/884893/en>.
- [24] Ruslan Salakhutdinov and Geoffrey Hinton. Deep boltzmann machines. In David van Dyk and Max Welling, editors, *Proceedings of the Twelfth International Conference on Artificial Intelligence and Statistics*, volume 5 of *Proceedings of Machine Learning Research*, pages 448–455, Hilton Clearwater Beach Resort, Clearwater Beach, Florida USA, 16–18 Apr 2009. PMLR.
- [25] Tobias Schröder, Zijing Ou, Yingzhen Li, and Andrew B Duncan. Energy-based modelling for discrete and mixed data via heat equations on structured spaces. *arXiv preprint arXiv:2412.01019*, 2024.
- [26] Truyen Tran, Dinh Q Phung, and Svetha Venkatesh. Mixed-variate restricted boltzmann machines. In *Proceedings of the Asian Conference on Machine Learning*, volume 20 of *Proceedings of Machine Learning Research*, pages 213–229. PMLR, 2011.
- [27] Yuichiro Tsutsui and Masafumi Hagiwara. Analog value associative memory using restricted boltzmann machine. *Journal of Advanced Computational Intelligence and Intelligent Informatics*, 23(1):60–66, 2019.
- [28] Princeton University. About wordnet. <https://wordnet.princeton.edu/>, 2010. Accessed: 2025-05-01.
- [29] Aaron van den Oord, Nal Kalchbrenner, and Koray Kavukcuoglu. Pixel recurrent neural networks, 2016.
- [30] Aaron van den Oord, Nal Kalchbrenner, Oriol Vinyals, Lasse Espeholt, Alex Graves, and Koray Kavukcuoglu. Conditional image generation with pixelcnn decoders, 2016.
- [31] William Whitehead, Zachary Nelson, Kerem Y. Camsari, and Luke Theogarajan. Cmos-compatible ising and potts annealing using single-photon avalanche diodes. *Nature Electronics*, 6(12):1009–1019, November 2023.
- [32] F. Y. Wu. The potts model. *Rev. Mod. Phys.*, 54:235–268, Jan 1982.